Supporting Information

Gadolinium-Chelated Conjugated Polymer-Based Nanotheranostics for Photoacoustic/Magnetic Resonance/NIR-II Fluorescence Imaging-Guided Cancer Photothermal Therapy

Xiaoming Hu,[a] Yufu Tang,[a] Yuxuan Hu,[b] Feng Lu,[a] Xiaomei Lu,[c] Yuqi Wang,[b] Jie Li,[a] Yuanyuan Li,[a] Yu Ji,[a] Wenjun Wang,[d] Deju Ye,[b] Quli Fan*[a] and Wei Huang[a, c, e]

[a]*Key Laboratory for Organic Electronics and Information Displays (KLOEID) & Institute of Advanced Materials (IAM), Jiangsu National Synergetic Innovation Center for Advanced Materials (SICAM), Nanjing University of Posts & Telecommunications, Nanjing 210023, China. E-mail: iamqlfan@njupt.edu.cn;*

[b]*State Key Laboratory of Analytical Chemistry for Life Science, School of Chemistry and Chemical Engineering, Nanjing University, Nanjing, 210093, China;*

[c]*Key Laboratory of Flexible Electronics (KLOFE) & Institute of Advanced Materials (IAM), Jiangsu National Synergetic Innovation Center for Advanced Materials (SICAM), Nanjing Tech University (NanjingTech), Nanjing 211816, China;*

[d]*Key Lab of Optical Communication Science and Technology of Shandong Province & School of Physics Science and Information Engineering, Liaocheng University, Liaocheng 252059, China;*

[e]*Shaanxi Institute of Flexible Electronics (SIFE), Northwestern Polytechnical University (NPU), Xi'an 710072, China.*

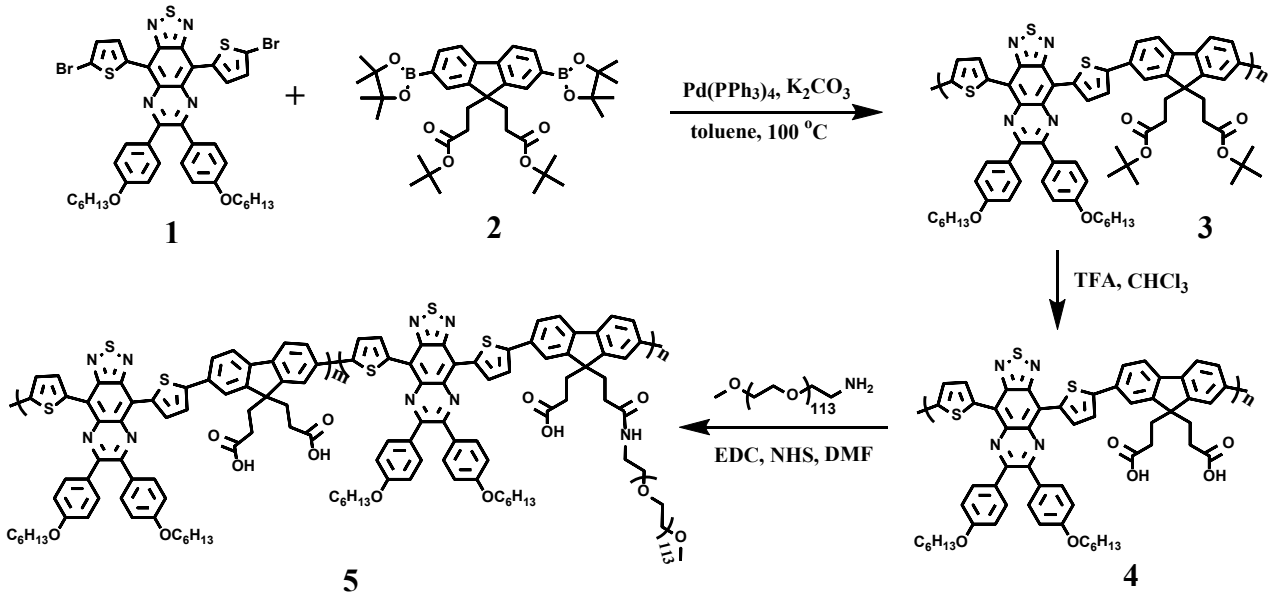

Scheme S1. Synthetic route to **PFTQ-PEG**.

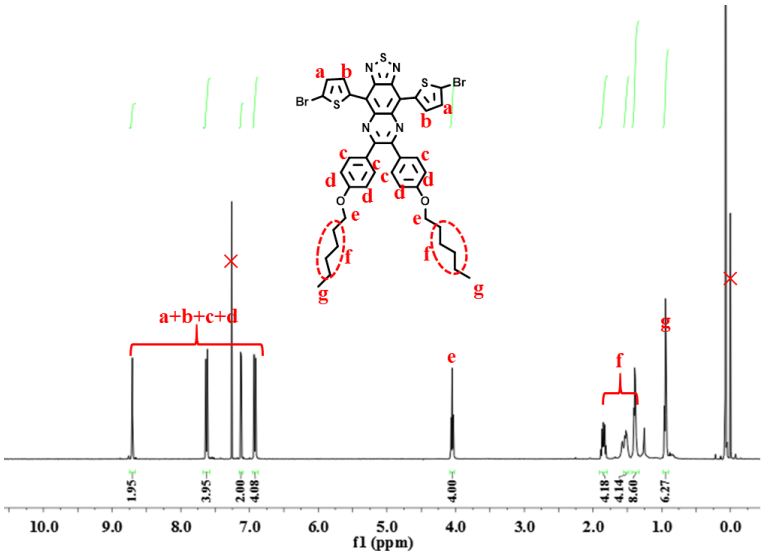

Figure S1. ^{1}H-NMR spectrum of **1**.

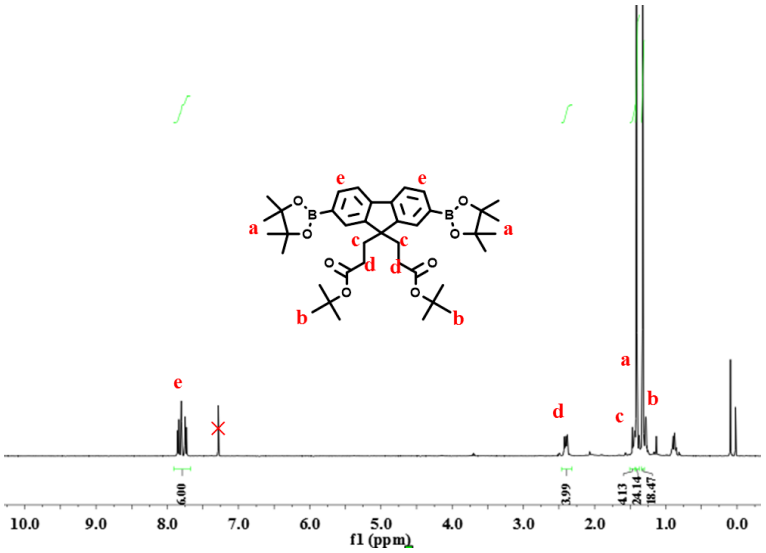

Figure S2. [1]H-NMR spectrum of **2**.

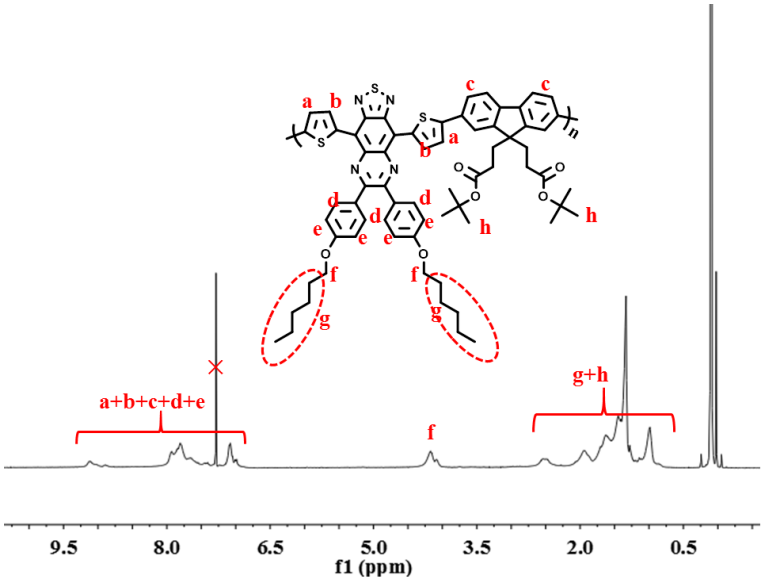

Figure S3. [1]H-NMR spectrum of **3** (PFTQ).

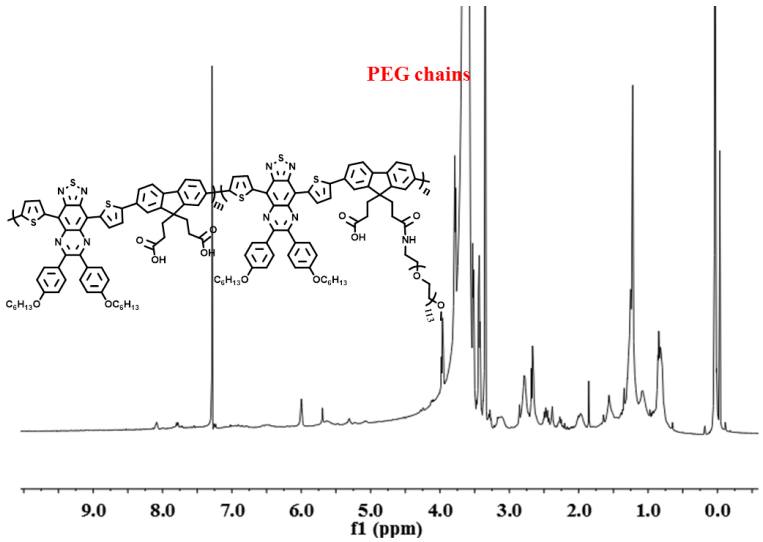

Figure S4. ^{1}H-NMR spectrum of **PFTQ-PEG**.

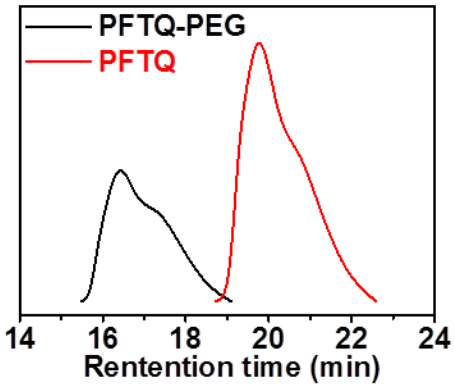

Figure S5. Gel permeation chromatography (GPC) curve of PFTQ and PFTQ-PEG.

Table S1. GPC date of PFTQ and PFTQ-PEG in THF eluent.

	Mn	Mw	Mw/Mn
PFTQ	43708	64961	1.49
PFTQ-PEG	84495	119277	1.41

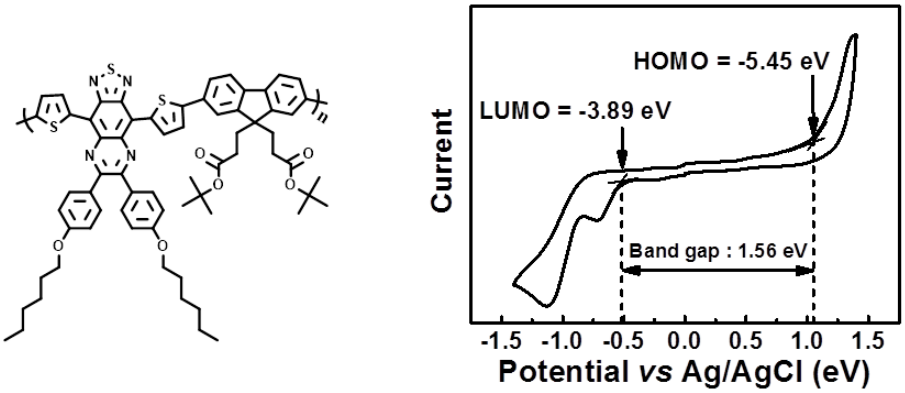

Figure S6. The cyclic voltammograms of the polymer (left) in dichloromethane.

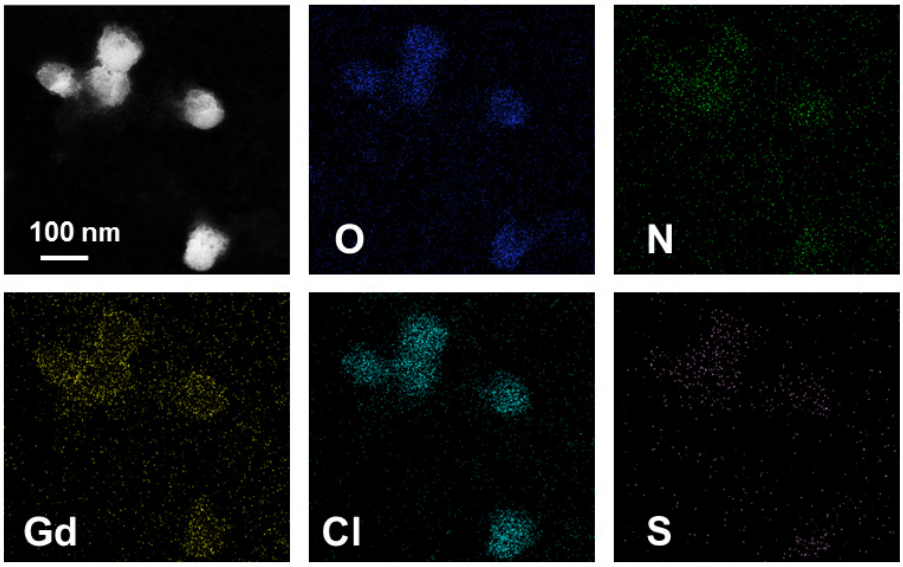

Figure S7. High-angle annular dark-field scanning TEM (HHAADF-STEM)-based elemental mapping of PFTQ-PEG-Gd NPs.

Physiological stability of PFTQ-PEG-Gd NPs

The hydrodynamic size distribution of PFTQ-PEG-Gd NPs in serum was performed to evaluate the stability of NPs in the biological environments. The PFTQ-PEG-Gd NPs (1 mg) were added to 50% fatal bovine serum (FBS, 5 mL) and 50% PBS (5 mL) and incubated at 37 °C for 48 h. The sample was analyzed at 0 h, 2 h, 4 h, and 24 h by DLS. As shown in Figure S8, all the hydrodynamic sizes of the

NPs still retained at approximately 138 nm and their polydispersities were not changed. No obvious change in hydrodynamic sizes suggests the excellent physiological stability of PFTQ-PEG-Gd NPs in biological environment.

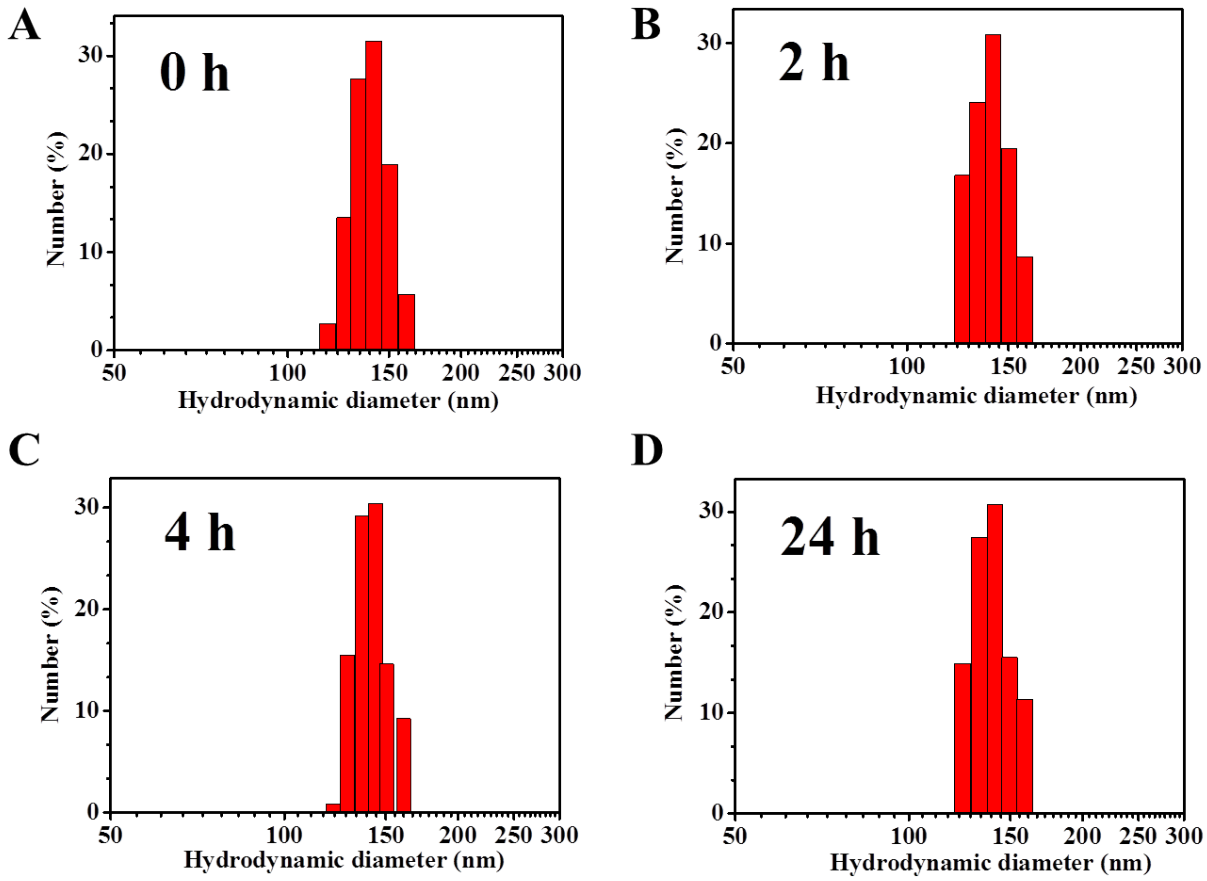

Figure S8. Stability of the PFTQ-PEG-Gd NPs hydrodynamic size during different incubation periods (0 h, 2 h, 4 h, 24 h) with serum.

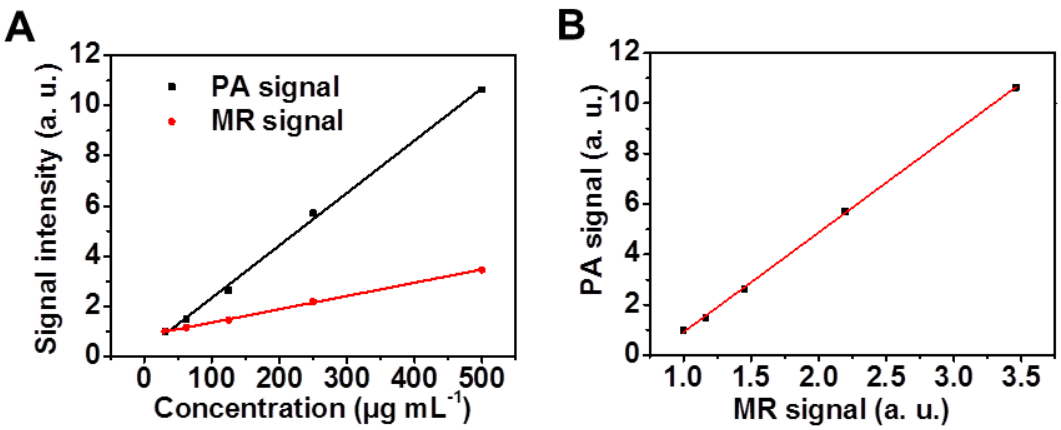

Figure S9. MRI-PAI signal correlation in vitro. (A) The relationship of MRI and photoacoustic signal with PFTQ-PEG-Gd concentration. (B) MR signal vs. PA signal.

We studied the relationship of MR versus PA signal intensity of the PFTQ-PEG-Gd NPs and they showed good linear relationship. In addition, the slope of increased MR signal intensity with different concentrations was lower than that of PA signal intensity, indicating that the PAI of PFTQ-PEG-Gd NPs was more sensitive than the MRI.

NIR-II fluorescence quantum yield measurement of PFTQ-PEG-Gd NPs

The NIR-II fluorescence quantum yield of the prepared PFTQ-PEG-Gd NPs was measured according to a previously published protocol which utilizes the dye IR-1061 whose quantum yield has been reported as 1.7% [1, 2]. In detail, a stock solution of 1 mg mL^{-1} IR-1061 in dichloromethane (DCM) was diluted in DCM until reaching an absorbance value of ~ 0.10 or less than 0.10 at 808 nm. A serial of diluent IR-1061 was performed, yielding a total of five solutions with absorbance values at 808 nm of 0.098818, 0.083751, 0.067779, 0.041690 and 0.024483, which shown in Figure S10A. NIR emission spectra of the five solutions were taken. The 808-nm laser was used as the excitation source and a 900-nm long-pass filter was used as the emission filter to acquire the emission spectrum (Figure S10B). Identical absorption and emission measurements were performed for PFTQ-PEG-Gd NPs in aqueous solutions (Figure S10D-E). All emission spectra were corrected after raw data acquisition to account for the detector sensitivity profile and the extinction features of the filters, and integrated in the objective region. The integrated fluorescence intensity was plotted against absorbance at 808 nm (the excitation wavelength) and fitted into a linear function (Figure S10C and S10F). Two slopes, one obtained for the IR-1061 DCM reference and the other

from the PFTQ-PEG-Gd NPs sample, were used in the calculation of the quantum yield of PFTQ-PEG-Gd NPs in water, according to the following equation:

$$QY_{sample} = QY_{ref} \times \frac{Slope_{sample}}{Slope_{ref}} \times \left(\frac{n_{sample}}{n_{ref}}\right)^2$$

where QY_{ref} is 1.7% and n_{sample} and n_{ref} are the refractive index of water and DCM, respectively. QY_{sample} was calculated to be **0.38%**. The quantum yield of PFTQ-PEG-Gd NPs was on par with the majority of NIR-II nano-materials, including carbon nanotubes, the most commonly used NIR-II fluorophore for in vivo imaging, and thus very suitable for in vivo imaging.

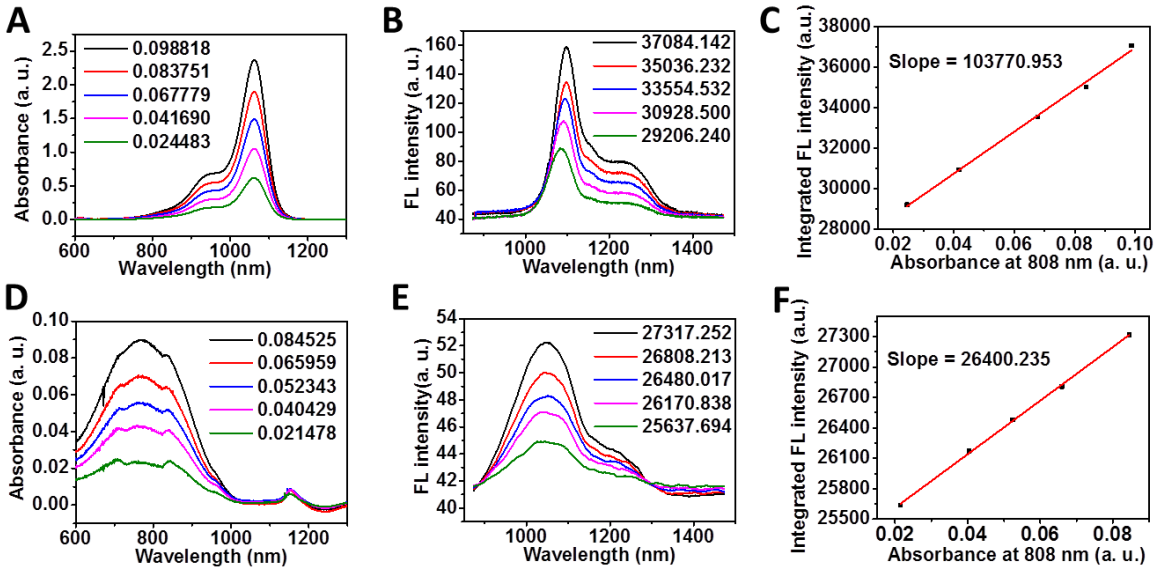

Figure S10. (A) The absorption spectra of different concentrations of IR-1061 in dichloromethane with absorbance values at 808 nm of 0.098818, 0.083751, 0.067779, 0.041690 and 0.024483. (B) The corresponding fluorescence spectra of above five solutions with absorbance values at 808 nm. (C) For all dichloromethane solutions of IR-1061, their absorbance values were then plotted versus area under curve, and fitted into a linear function, where slope of the fitted line was read as insert. The same absorption (D) and emission (E) measurements were performed for PFTQ-PEG-Gd NPs in aqueous solutions. (F) Area under curve in the emission spectrum of each solution of PFTQ-PEG-Gd

NPs was then plotted against their absorbance at 808 nm and fitted into a linear function, as slope was indicated.

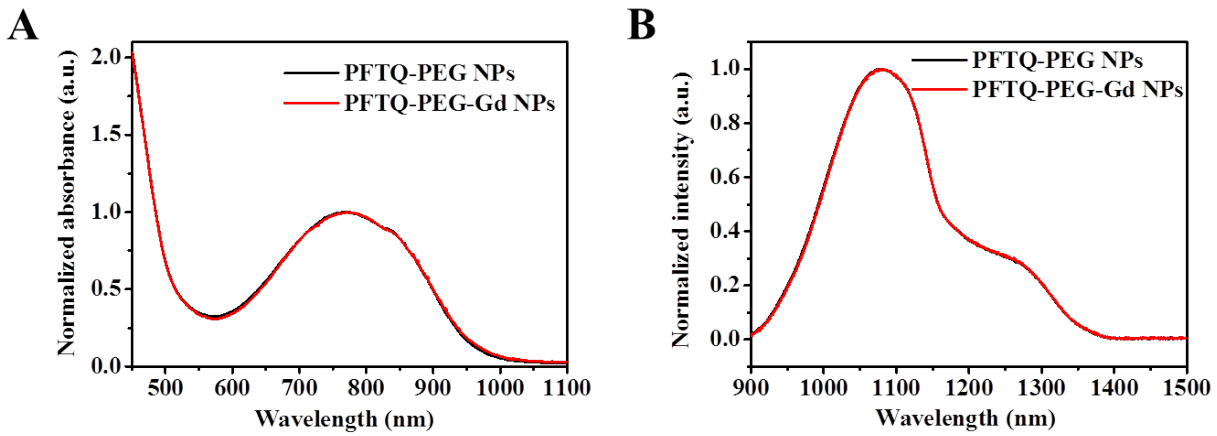

Figure S11. (A) Absorbance and (B) fluorescent emission spectra of PFTQ-PEG NPs and PFTQ-PEG-Gd NPs in water.

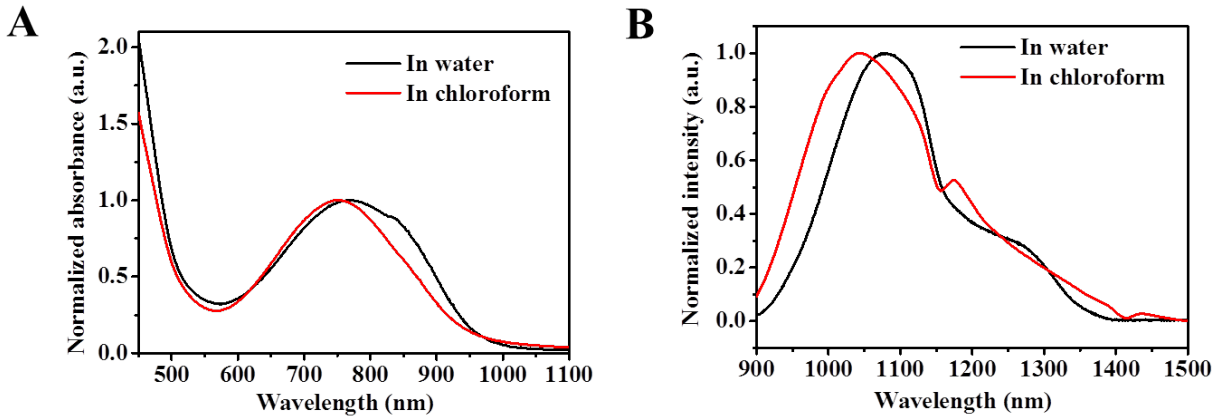

Figure S12. (A) Absorbance and (B) fluorescent emission spectra of PFTQ-PEG NPs in water and chloroform.

Calculation of photothermal conversion efficiency of PFTQ-PEG-Gd NPs

Photothermal conversion efficiency of PFTQ-PEG-Gd NPs was calculated by recording the temperature variation of the aqueous solution of the NPs as a function of time under a continuous

808 nm laser (1.0 W cm^{-2}) until the solution reached a steady-state temperature [3]. The photothermal conversion efficiency (η) was calculated according to equation:

$$\eta = \frac{hA\Delta T_{max} - Q_{dis}}{I(1 - 10^{-A_{808}})}$$

h: the heat transfer coefficient

A: the surface area of the container

*ΔT_{max}: the increased maximum steady-state temperature (62.4-24.7=**37.7**)*

Q_{dis}: the heat dissipation from the light absorbed by water and the sample cell

*I: laser power (**1.0 W cm^{-2}**)*

*A_{808}: the absorbance of the NPs at 808 nm (**0.60347**)*

The value of **hA** was calculated according to equation:

$$\tau = \frac{m_D c_D}{hA}$$

τ: the time constant for heat transfer of system which was determined to be τ = 210.15 from **Figure S13B**

m_D: the mass of the water (0.3 g)

c_D: the heat capacity (4.2 J g^{-1}) of the water

hA was calculated to be **0.005996**

Q_{dis} was calculated to be **0.034** according to equation:

$$Q_{dis} = \frac{m_D c_D (T_{\max(water)} - T_{surr})}{\tau_{water}}$$

$T_{max(water)}$: 29.1

T_{surr}: 24.8

τ_{water}: 158.75

So according to the obtained date and above equations, the photothermal conversion efficiency (η) of PFTQ-PEG-Gd NPs was calculated to be **26%**.

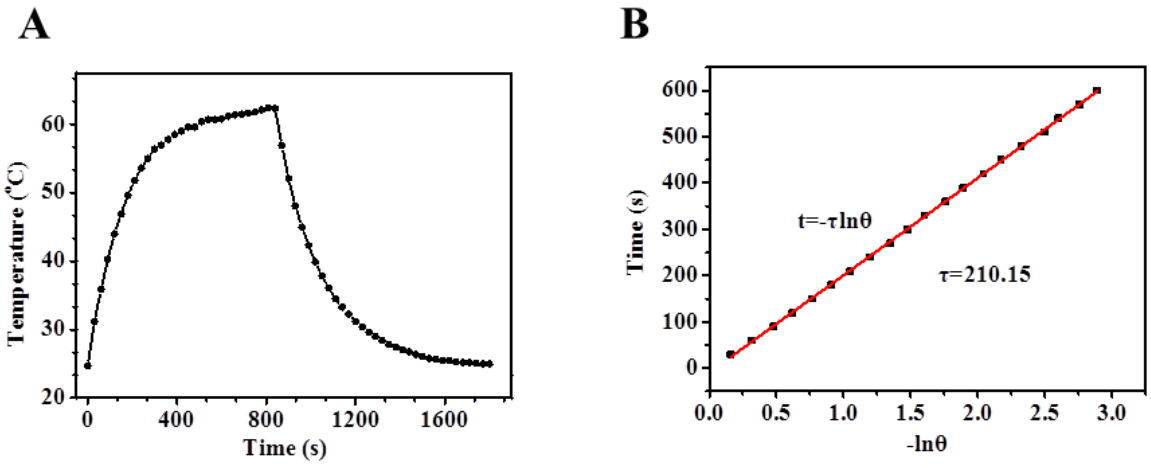

Figure S13. (A) Photothermal effect of PFTQ-PEG-Gd NPs aqueous solution when radiated by an 808 nm laser (1 W cm^{-2}). The laser was removed after irradiating the sample. (B) The time versus the negative natural logarithm of the temperature from the cooling test.

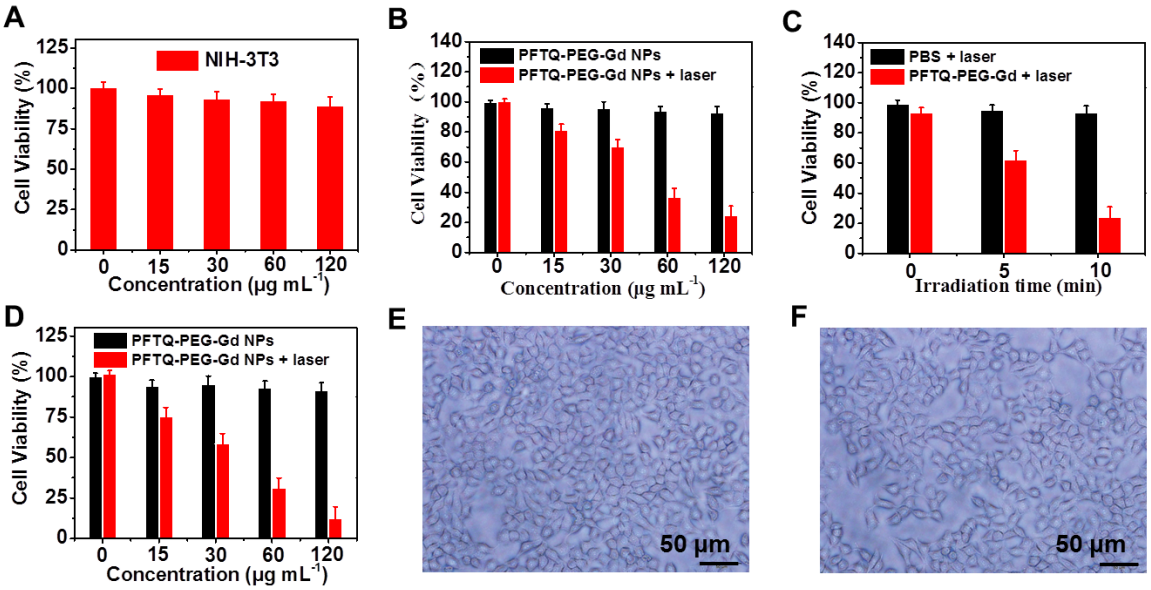

Figure S14. (A) MTT assay using NIH-3T3 cells with PFTQ-PEG-Gd NPs concentration 0, 15, 30, 60 and 120 μg mL^{-1} after 24 h incubation at 37 °C. (B) Relative viabilities of 4T1 cells for different treatment groups after being incubated with PFTQ-PEG-Gd NPs with different concentrations. (C)

the cell viability of 4T1 cells cultured with PFTQ-PEG-Gd NPs as a function of laser irradiation time. (D) Relative viabilities of Hela cells for different treatment groups after being incubated with PFTQ-PEG-Gd NPs with different concentrations. The representative phase-contrast photomicrographs of Hela cells cultured with (E) PBS and (F) PFTQ-PEG-Gd NPs of 120 μg mL^{-1}.

In Vitro Hemocompatibility

In vitro hemocompatibility was evaluated as follows: a KM mouse was anesthetized and heart punctured to collect blood. After removing the serum via centrifugation, mouse red blood cells (mRBCs) were collected and stored in saline at 4 °C for further use. Then, 0.2 mL of the mRBCs suspension was treated with 0.8 mL water (control) or different concentrations (0.2, 0.4, 0.8, and 1 mg mL^{-1} in saline) of PFTQ-PEG-Gd NPs in a 1.5-mL Eppendorf tube at 37 °C for 2 h (n=3). Then, the treated mRBCs were centrifuged (10000 rpm, 1 min) to harvest the supernatant. The absorbance at 541 nm of supernatant from samples treated with microfibers (D_t), water (D_{pc}), and saline (D_{nc}) were recorded using Lambda 25 UV–vis spectrophotometer. The hemolytic percentage (HP) can be calculated as followed.

$$\mathrm{HP}(\%) = \frac{D_t - D_{nc}}{D_{pc} - D_{nc}} \times 100\%$$

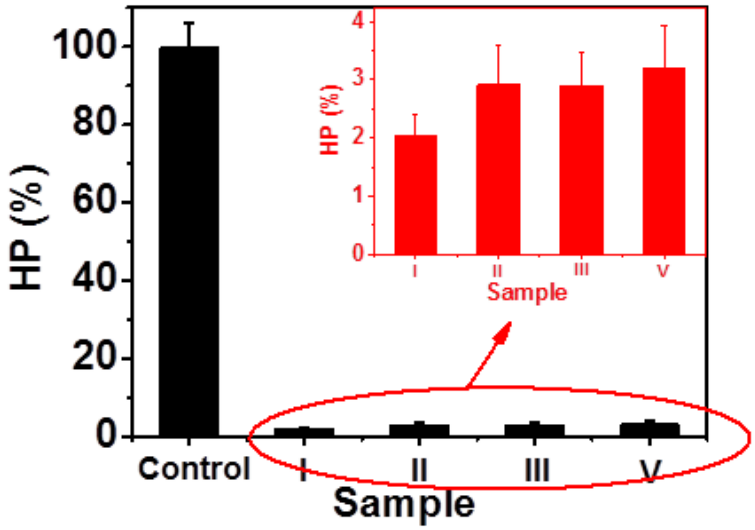

Figure S15. Hemolytic assay of water (control) and PFTQ-PEG-Gd NPs with different concentrations (I: 0.2 mg mL^{-1}, II: 0.4 mg mL^{-1}, III: 0.8 mg mL^{-1} and V: 1 mg mL^{-1}). The HP of mRBCs treated with each kind of PFTQ-PEG-Gd NPs was lower than 5%, indicating that the NPs possessed an excellent in vitro hemo-compatibility. By contrast, mRBCs treated with water were completely destroyed.

In Vivo Hemocompatibility

In vivo hemo-compatibility was studied in the Laboratory Animal Center of Jiangsu KeyGEN BioTECH Corp., Ltd. The healthy KM mice (n = 3 for each group) that were intravenously injected with PFTQ-PEG-Gd NPs (150 μL, 1 mg mL^{-1}) were anesthetized on 1, 4 and 7 days for cardiac puncturing to collect blood. KM mice treated with PBS were tested as control. The routine blood parameters included red blood cells (RBC), white blood cells (WBC), platelets (PLT), hematocrit (HCT), mean corpuscular volume (MCV), mean corpuscular hemoglobin (MCH), mean corpuscular hemoglobin concentration (MCHC), and hemoglobin (HGB).

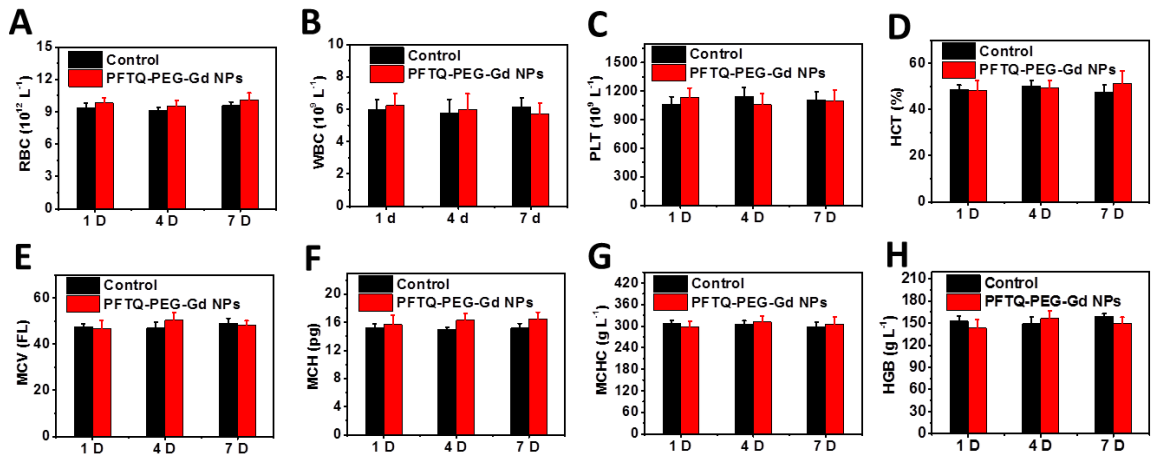

Figure S16. Blood routine examination results of mice treated with saline (control) and PFTQ-PEG-Gd NPs for 1, 3 and 7 days. Compared with the control group, all the parameters in the PFTQ-PEG-Gd NPs treated groups at all-time points did not show any significant differences, indicating that the NPs do not cause obvious infection and inflammation in the treated mice.

In vivo blood elimination kinetics of PFTQ-PEG-Gd NPs

For in vivo pharmacokinetic study, healthy Balb/c mice were randomly divided into two groups (n = 3 for each group). Group (i): the commercial Gd-DTPA (Gd content: 150 μL, 200 μg mL^{-1}) contrast agent and group (ii): PFTQ-PEG-Gd NPs (Gd content: 150 μL, 200 μg mL^{-1}). After intravenous injection of Gd-DTPA or PFTQ-PEG-Gd NPs, about 10 - 15 μL of blood was drawing from the mouse tail vein at different time-intervals post injection. Each blood sample was weighted and then dissolved in aqua regia. The obtained homogeneous solution was then diluted with deionized water. The concentrations of Gd^{3+} in the blood samples were measured by inductively coupled plasma mass spectrometry (ICP-MS).

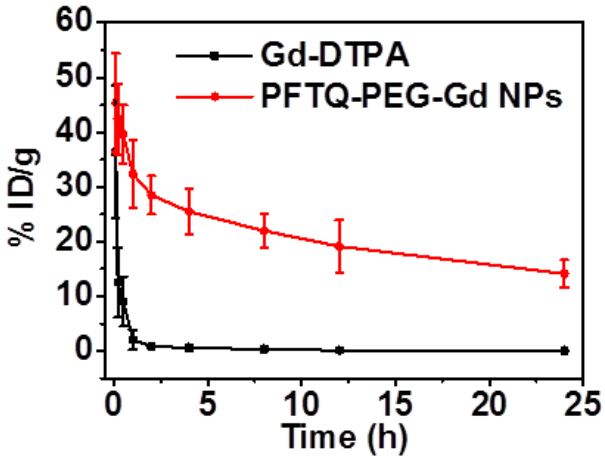

Figure S17. In vivo blood elimination kinetics of commercial Gd-DTPA contrast agent and PFTQ-PEG-Gd NPs. Compared to the commercial Gd-DTPA contrast agents, the PFTQ-PEG-Gd NPs possessed the prolonged blood circulation, which provided a guarantee for effective tumor accumulation of the NPs.

REFERENCES

1. Tao Z, Hong G, Shinji C, Chen C, Diao S, Antaris AL, et al. Biological imaging using nanoparticles of small organic molecules with fluorescence emission at wavelengths longer than 1000 nm. Angew Chem Int Ed. 2013; 52: 13002-6.

2. Casalboni M, De Matteis F, Prosposito P, Quatela A, Sarcinelli F. Fluorescence efficiency of four infrared polymethine dyes. Chem Phys Lett. 2003; 373: 372-8.

3. Zhang S, Guo W, Wei J, Li C, Liang XJ, Yin M. Terrylenediimide-based intrinsic theranostic nanomedicines with high photothermal conversion efficiency for photoacoustic imaging-guided cancer therapy. ACS Nano. 2017; 11: 3797-805.